

## MHD Free Convection within Trapezoidal Cavity with Uniformly Heated Bottom Wall

Muhammad Sajjad Hossain<sup>1\*</sup> and Mohammad Abdul Alim<sup>2</sup>

<sup>1</sup>Department of Arts and Sciences, Ahsanullah University of Science & Technology  
Dhaka-1208, Bangladesh

\*Corresponding author's Email: [msh80\\_edu@yahoo.com](mailto:msh80_edu@yahoo.com)

<sup>2</sup>Department of Mathematics, Bangladesh University of Engineering & Technology  
Dhaka-1000, Bangladesh  
Email: [a0alim@gmail.com](mailto:a0alim@gmail.com)

*Received 30 March 2013; accepted 22 April 2013*

**Abstract.** Numerical simulation of two-dimensional laminar steady-state on MHD free convection for heat flow patterns with heatlines concept within trapezoidal cavity has been investigated. In this study, free convection within a trapezoidal enclosure for uniformly heated bottom wall, insulated top wall and isothermal side walls with inclination angles ( $\phi$ ) are considered. The fluid is concerned for the wide range of Rayleigh number ( $Ra$ ) from  $10^3$  to  $10^7$  and Prandtl number ( $Pr$ ) from 0.026-1000 with various tilt angles  $\Phi = 45^\circ, 30^\circ$  and  $0^\circ$ (square). The properties of the fluid were presumed to be constant. The physical problems are represented mathematically by different sets of governing equations along with the corresponding boundary conditions. The non-dimensional governing equations are discretized by using Galerkin weighted residual method of finite element formulation. Results are presented in terms of streamlines, isotherms, average and Local Nusselt numbers, for different parameters namely Prandtl number  $Pr$  and Rayleigh number  $Ra$ . This range of  $Ra$  is selected on the basis of calculation covering free convection dominated regimes. The results indicate that the Local and average Nusselt number at the uniform heating of bottom wall of the cavity depends on the dimensionless parameters.

**Keywords:** Free convection, finite element method, Trapezoidal cavities, Uniform heating.

**AMS Mathematics Subject Classification (2010):** 76Dxx, 76D99, 76E09

<b>Nomenclature</b>		$v$	y component of velocity (m/s)
		$V_0$	Lid velocity
$B_0$	Magnetic induction	$x, y$	Cartesian coordinates
$C_p$	Specific heat at constant pressure (J/kg K)	$X, Y$	Dimensionless Cartesian coordinates
$G$	Gravitational acceleration (m/s <sup>2</sup> )	$T_h$	Heated uniformly
$Gr$	Grashof number	$T_c$	Cold temperature
$H$	Convective heat transfer coefficient (W/m <sup>2</sup> K)	<b>Greek symbols</b>	
$Ha$	Hartmann number	$\alpha$	Thermal diffusivity (m <sup>2</sup> /s)
$K$	Thermal conductivity of fluid (W/m K)	$\beta$	Coefficient of thermal expansion (K <sup>-1</sup> )
$L$	Height or base of trapezoidal cavity (m)	$\rho$	Density of the fluid (kg/m <sup>3</sup> )
$K$	Thermal conductivity ratio fluid	$\Delta\theta$	Temperature difference
$N$	Total number of nodes	$\Theta$	Fluid temperature
$Nu_{av}$	Average Nusselt number	$\mu$	Dynamic viscosity of the fluid (Pa s)
$Nu_{local}$	Local Nusselt number	$\Pi$	Heatfunction
$P$	Non-dimensional pressure	$\nu$	Kinematic viscosity of the fluid (m <sup>2</sup> /s)
$p$	Pressure	$\sigma$	Fluid electrical conductivity ( $\Omega^{-1}m^{-1}$ )
$Pr$	Prandtl number	<b>Subscripts</b>	
$Ra$	Rayleigh number	$b$	Bottom wall
$T$	Non-dimensional temperature	$l$	Left wall
$T_h$	Temperature of hot bottom wall (k)	$r$	Right wall
$T_c$	Temperature of cold bottom wall (k)	$s$	Side wall
$U$	x component of dimensionless velocity		
$u$	x component of velocity (m/s)		
$V$	y component of dimensionless velocity		

## 1. Introduction

Free convection flow and heat transfer in a trapezoidal cavity have been the topic of many researches in engineering studies. These studies consist of various technological applications such as in electronic cooling, ventilation of building, design of solar collectors etc. Most of the cavities commonly used in industries are cylindrical, rectangular, trapezoidal, triangular etc. Trapezoidal cavities have

### MHD Free Convection within Trapezoidal Cavity with Uniformly Heated Bottom

received a considerable attention for its application in various fields. A brief review of the relevant literature is presented in the following section.

Anandalakshmi and Basak [1] studied for the energy distribution and thermal mixing in steady laminar natural convective flow through the rhombic enclosures with various inclination angles ( $\varphi$ ) for various industrial applications. Also an analysis on entropy generation during natural convection in a trapezoidal cavity with various inclination angles ( $\varphi = 45^\circ, 60^\circ$  and  $90^\circ$ ) has been carried out for an efficient thermal processing of various fluids of industrial importance ( $Pr = 0.015, 0.7$  and  $1000$ ) in the range of Rayleigh number ( $10^3 - 10^5$ ) by Basak et al. [2]. Basak et al. [3] studied a comprehensive heatline based approach for natural convection flows in trapezoidal enclosures with the effect of various walls heating. Basak et al. [4] also presented natural convection flows in porous trapezoidal enclosures with various inclination angles. Natural convection in trapezoidal enclosures for uniformly heated bottom wall, linearly heated vertical wall(s) in presence of insulated top wall have been investigated numerically with penalty finite element method by Basak et al. [5]. Basak et al. [6] also performed the phenomena of natural convection within a trapezoidal enclosure filled with porous matrix for linearly heated vertical wall(s) with various inclination angles  $\varphi$ . Basak et al. [7] also studied the phenomena of natural convection in a trapezoidal enclosure filled with porous matrix numerically. Besides, a study of the natural heat and mass transfer in a trapezoidal cavity heated from the bottom and cooled from the inclined upper wall is undertaken by Boussaid et al. [8]. He obtained results which show that the flow configuration depends on the  $\theta$  angle inclination of the upper wall. Peric [9] studied Natural convection in trapezoidal cavities with a series of symmetrically refined grids  $10 \times 10$  to  $160 \times 160$  control volume and observed the convergence of results for grid independent solutions. A penalty finite element analysis with bi-quadratic elements is performed to investigate the influence of uniform and non-uniform heating of bottom wall on natural convection flows in a trapezoidal cavity by Natarajan et al. [10]. Natarajan et al. [11] presented a numerical study of combined natural convection and surface radiation heat transfer in a solar trapezoidal cavity absorber for Compact Linear Fresnel Reflector (CLFR). The numerical simulation results are presented in terms of Nusselt number correlation to show the effect of these parameters on combined natural convection and surface radiation heat loss. Saleh et al. [12] also studied the effect of a magnetic field on steady convection in a trapezoidal enclosure filled with a fluid-saturated porous medium by the finite difference method. Hung et al. [13] made an attempt to analyze the nonlinear instability of a magnetohydrodynamics (MHD) film flow with phase change at the interface. They pointed that increasing the stability of film flow by controlling magnetic field; a film flow with optimum conditions could be obtained. Basak et al. [14] also investigated heat flow patterns in the presence of natural convection within trapezoidal enclosures with heatlines concept. In this study, natural convection within a trapezoidal enclosure for uniformly and non-uniformly heated bottom wall, insulated top wall and isothermal side walls with inclination angle have been investigated.

However, visualization of heat flows via heatlines for magnetohydrodynamics with uniformly heated bottom walls were not reported for

trapezoidal enclosures. It is also essential to study the heat transfer characteristics in complex geometries in order to obtain the optimal design of the container for various industrial applications. The aim of the present work is to present the effects on heat flow via heatlines for MHD free convection within trapezoidal cavity with uniformly heated bottom wall. Results will be presented for different non-dimensional governing and physical parameters in terms of streamlines, stream functions, total heat flux, isotherms, heat transfer rate as well as the average temperature of the fluid in the cavity. The heatlines and thermal mixing will be illustrated for commonly used fluid with  $Pr = 0.026 - 1000$  and  $Ra = 10^3 - 10^7$  in various industrial applications.

## 2. Problem Definition

The physical model is shown in Figure 1, along with the important geometric parameters. A trapezoidal cavity of height  $L$  with the left wall inclined at an angle  $\phi = 45^\circ, 30^\circ, 0^\circ$  with  $Y$  axis is considered. The heat transfer and the fluid flow for uniform heating in a two-dimensional trapezoidal cavity with a fluid whose left wall and right wall (i.e. side walls) are subjected to cold  $T_c$  temperature, bottom wall is subjected to hot  $T_h$  temperature while the top wall is kept insulated. The boundary conditions for velocity are considered as no-slip on solid boundaries.

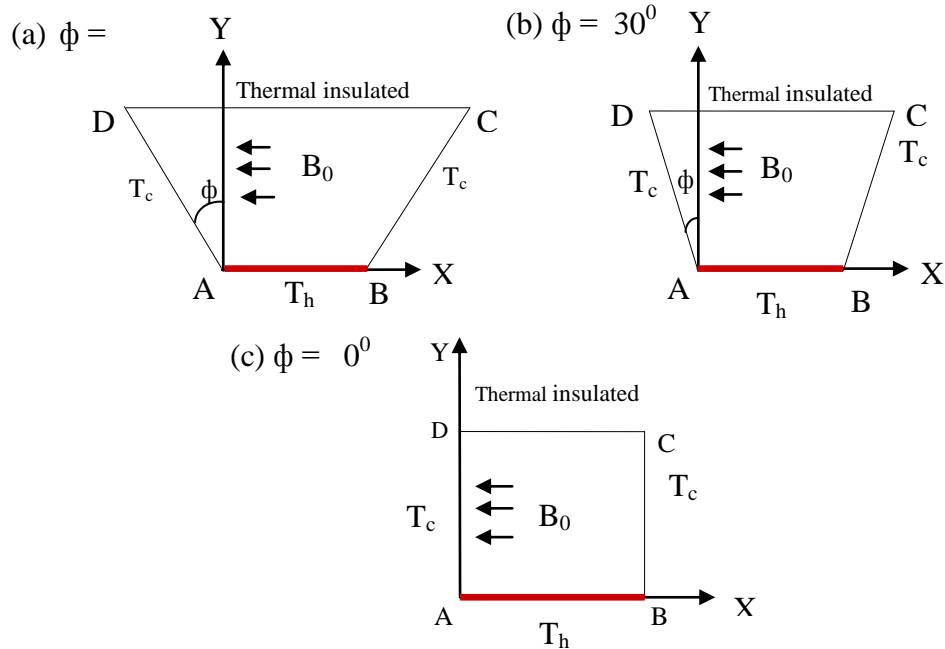


**Figure 1:** Schematic diagram of the physical system for (a)  $\phi = 45^\circ$ , (b)  $\phi = 30^\circ$  and (c)  $\phi = 0^\circ$

## 3. Governing equations

The following assumptions are made: the fluid is steady, two-dimensional, laminar incompressible and Newtonian, there is no viscous dissipation. For the treatment of the buoyancy term in the momentum equation, Boussinesq approximation is

### MHD Free Convection within Trapezoidal Cavity with Uniformly Heated Bottom

employed for the variations of density and buoyancy force is included as a body force in the  $v$ -momentum equation.

Using non-dimensional variables defined below, the non-dimensional governing equations are obtained as:

$$\frac{\partial U}{\partial X} + \frac{\partial V}{\partial Y} = 0 \quad (1)$$

$$U \frac{\partial U}{\partial X} + V \frac{\partial U}{\partial Y} = -\frac{\partial P}{\partial X} + \text{Pr} \left( \frac{\partial^2 U}{\partial X^2} + \frac{\partial^2 U}{\partial Y^2} \right) \quad (2)$$

$$U \frac{\partial U}{\partial X} + V \frac{\partial U}{\partial Y} = -\frac{\partial P}{\partial Y} + \text{Pr} \left( \frac{\partial^2 V}{\partial X^2} + \frac{\partial^2 V}{\partial Y^2} \right) + Ra \text{Pr} \theta - Ha^2 \text{Pr} V \quad (3)$$

$$U \frac{\partial \theta}{\partial X} + V \frac{\partial \theta}{\partial Y} = \left( \frac{\partial^2 \theta}{\partial X^2} + \frac{\partial^2 \theta}{\partial Y^2} \right) \quad (4)$$

Non-dimensional variables used for the above equations (1-4) stated as follows:

$$X = \frac{x}{L}, \quad Y = \frac{y}{L}, \quad U = \frac{uL}{\alpha}, \quad V = \frac{vL}{\alpha}, \quad P = \frac{pL^2}{\rho\alpha^2}, \quad \theta = \frac{T - T_c}{T_h - T_c}, \quad \text{Pr} = \frac{\nu}{\alpha},$$

$$Gr = \frac{g\beta L^3 (T_h - T_c)}{\nu^2}, \quad Ra = \frac{g\beta L^3 (T_h - T_c) \text{Pr}}{\nu^2}, \quad Ha^2 = \frac{\sigma B_0^2 L^2}{\mu}, \quad \alpha = \frac{k}{\rho C_p}$$

The appropriate boundary conditions (also shown in Fig. 1) used to solve the equations (1)-(4) can be written as:

At the bottom wall:

$$U = 0, \quad V = 0, \quad \theta = 1 \quad \forall Y = 0, \quad 0 \leq X \leq 1$$

At the left wall:

$$U = 0, \quad V = 0, \quad \theta = 0, \quad \forall X \cos \phi + Y \sin \phi = 0, \quad 0 \leq Y \leq 1$$

At the right wall:

$$U = 0, \quad V = 0, \quad \theta = 0, \quad \forall X \cos \phi - Y \sin \phi = \cos \phi, \quad 0 \leq Y \leq 1$$

At the top wall:

$$U = 0, \quad V = 0, \quad \frac{\partial \theta}{\partial Y} = 0, \quad \forall Y = 1, \quad -\tan \phi \leq X \leq (1 + \tan \phi)$$

The local Nusselt number at the heated surface of the cavity which is defined by the following expression:

$$Nu_l = Nu_r = Nu_b = Nu_s = -\frac{\partial \theta}{\partial n} \quad \text{where } n \text{ denotes the normal direction on a plane.}$$

The average Nusselt number at the heated bottom wall, cold left and right walls and insulated top walls of the cavity based on the non-dimensional variables may be

$$\text{expressed as: } Nu = \int_0^1 Nu_l dX = \int_0^1 Nu_r dX = \int_0^1 Nu_s dX = \int_0^1 Nu_b dX$$

#### 4. Finite Element Technique

The numerical procedure used in this work is based on the Galerkin weighted residual method of finite element formulation. The application of this technique is well described by Taylor and Hood [15] and Dechaumphai [16]. In this method, the solution domain is discretized into finite element meshes, which are composed of triangular elements. Then the nonlinear governing partial differential equations i.e., mass, momentum and energy equations are transferred into a system of integral equations by applying Galerkin weighted residual method. The integration involved in each term of these equations is performed by using Gauss quadrature method. Then the nonlinear algebraic equations so obtained are modified by imposition of boundary conditions. These modified nonlinear equations are transferred into linear algebraic equations by using Newton's method. Finally, these linear equations are solved by using Triangular Factorization method.

#### 5. Grid Independence Test

Seven different grid sizes of 6402, 12922, 14729, 15731, 25462, 26185, 26903 nodes and 952, 1947, 2218, 2363, 3852, 3960, 4071 elements respectively are chosen for the present simulation to test the independency of the results with the grid variations. Average Nusselt number at the heated surface study is performed for a trapezoidal cavity with  $Pr = 0.7$ ,  $\phi = 0$  and  $Ra = 10^5$ . From these values, a grid size of 15731 nodes and 2363 elements are chosen for better accuracy in Table 1.

Nodes (Elements)	6402 (952)	12922 (1947)	14729 (2218)	15731 (2363)	25462 (3852)	26185 (3960)	26903 (4071)
$Nu_{av}$	5.753017	6.120885	6.005761	6.123839	6.618788	6.74774	6.721055
Time (s)	3.563	6.813	7.235	7.875	13.781	14.0	14.266

**Table 1:** Grid Sensitivity Check at  $Pr = 0.7$ ,  $\phi = 0$ ,  $Ha = 50$  and  $Ra = 10^5$ .

#### 6. Code Validation

The work has been validated against the work of Basak et al. (March 2009) for natural convection in a trapezoidal cavity. Average Nusselt number is calculated for three different Rayleigh numbers ( $Ra = 10^3$ ,  $10^4$  and  $10^5$ ) and three different angles  $\phi = 45^\circ$ ,  $30^\circ$ ,  $0^\circ$ , while the prandtl number is fixed i.e.  $Pr = 0.7$  for uniform heating of bottom respectively in Table 2. The present average Nusselt numbers are in good agreement with these of Basak et al. (March 2009).

$Ra$	Average Nusselt Number, ( $Nu_{av}$ )					
	Present work			Basak et al. (2009)		
	$\phi = 0^\circ$	$\phi = 30^\circ$	$\phi = 45^\circ$	$\phi = 0^\circ$	$\phi = 30^\circ$	$\phi = 45^\circ$
$10^3$	6.055778	4.714051	3.894428	5.31956	3.93605	3.34577

MHD Free Convection within Trapezoidal Cavity with Uniformly Heated Bottom

$10^4$	6.09068	4.935452	4.19254	6.4311	5.37306	4.90481
$10^5$	7.558405	6.633036	5.952502	8.71198	7.80227	7.37514

**Table 2:** Code validation for uniform heating of bottom wall with  $Pr = 0.7$ .

## 7. Results and Discussion

Numerical studies have been studied on MHD free convection within trapezoidal cavity with uniformly heated bottom. In this endorsement uniformly heated bottom wall, thermal insulation of top wall and cold side (left or right) walls have been analyzed. Results are obtained on uniform heating for parametric study for the wide range of Rayleigh number,  $Ra = 10^3 - 10^7$  and Prandtl number,  $Pr = 0.026, 0.7, 1000$  with various angles,  $\phi = 45^\circ, 30^\circ, 0^\circ$  (square cavity).

### 7.1 Uniform Heating of Bottom Wall

Figures 2-7 display the effects of streamline (stream function), isotherms (temperature) and heatlines for  $Pr = 0.026, 0.7, 1000$  when bottom wall is uniformly heated and side walls is maintained as cold. Here we see that from the middle portion of the bottom wall fluid rise up and the fluid near the hot bottom wall has lower density. So it moves upward relatively heavy fluid along two vertical side walls moves downwards (flow down) forming symmetric rolls with clockwise and anticlockwise rotations inside the cavity and the fluid is heated up. Thus fluid completes circulation.

Figure 2 illustrates that the magnitudes of streamfunction contours are considerably smaller which express that, at low Rayleigh number the flow is primarily due to conduction. For  $Ra = 10^3$ ,  $Pr = 0.026$  and  $\phi = 0^\circ$  (square cavity) isotherms (temperature) with  $\theta = 0.05 - 0.10$  occur symmetrically along side (left or right) walls and with  $\theta \geq 0.15$  are smooth curves symmetric with respect to vertical symmetrical line (Fig. 2a). For  $Ra = 10^3$ ,  $Pr = 0.026$  and  $\phi = 30^\circ$  the temperature contours with  $\theta = 0.05 - 0.25$  occur symmetrically near the side walls of the enclosure and with  $\theta \geq 0.30$  are smooth curves symmetric with respect to central symmetrical line (Fig. 2b). Again for  $Ra = 10^3$ ,  $Pr = 0.026$  and  $\phi = 45^\circ$  isotherms (temperature) with  $\theta = 0.05 - 0.30$  occur symmetrically near the side walls of the enclosure and with  $\theta \geq 0.35$  are smooth curves symmetric with respect to vertical symmetrical line (Fig. 2c). The presence of significant convection is also exhibited with temperature distribution for various  $\phi$  in trapezoidal cavity. It can be explained with distribution of heat energy is governed by heat function or heat flux. Heatlines or total heat flux are shown in panels of fig.2a-c. Heatlines illustrate that heat energy from the bottom wall symmetrically distributed to side walls for various tilt angles of  $\phi$  especially for smaller  $Ra$ .

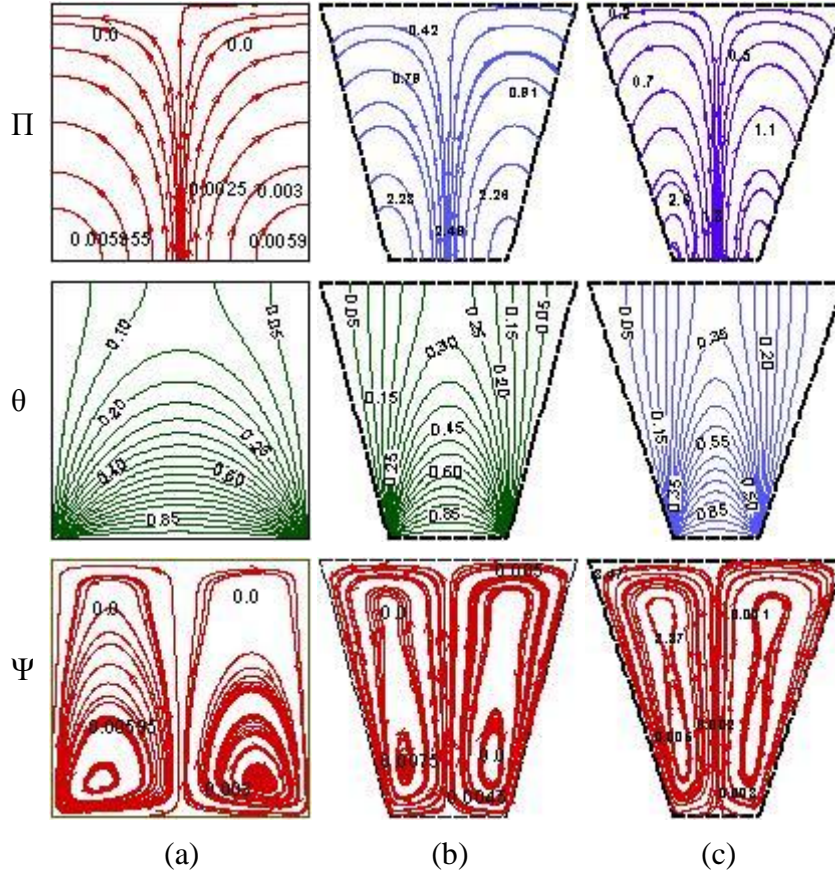


**Figure 2:** Stream function ( $\Psi$ ), temperature ( $\theta$ ), heat function or total heat flux( $\Pi$ ) contours for uniform bottom heating  $\theta(X,0) = 1$  with  $Pr = 0.026$ ,  $Ha = 50$  and  $Ra = 10^3$  (a)  $\Phi = 0^\circ$  (b)  $\Phi = 30^\circ$  (c)  $\Phi = 45^\circ$

It is important to note that two bottom corner edges have infinite heat flux as the cold wall is directly in contact with the hot bottom wall and sign of heat functions depend on boundary conditions at two bottom corners. Our sign convention is based on the fact that heat flow occurs from hot to cold walls and the positive heat flow corresponds to anticlockwise heat flow. It may be noted that the magnitudes of heat functions decrease from the bottom edges to the central symmetric line where no heat flux condition is valid due to symmetric boundary conditions for temperature.

Figure 3 illustrates that effect of buoyancy force is compared to viscous forces and the intensity of fluid motion has been increased by larger magnitudes of streamfunction for  $Ra = 10^7$ ,  $Pr = 0.026$ . The enhanced convection causes larger heat energy to flow from the bottom wall to the top portion of the vertical wall and large regime of the top portion of the cavity remains at uniform temperature for  $\phi = 45^\circ$  and  $30^\circ$ . It is interesting to note that isotherms are more compressed near to corners of bottom wall. Therefore the deformation occurs in the streamfunction near to the corners of bottom wall. As a result secondary circulations are also developed near to

### MHD Free Convection within Trapezoidal Cavity with Uniformly Heated Bottom

the intersection of uniformly heated bottom wall and center of the cold side walls for  $\phi = 0^\circ$  and for  $\phi = 30^\circ, 45^\circ$  symmetric multiple circulations near to corner appear.

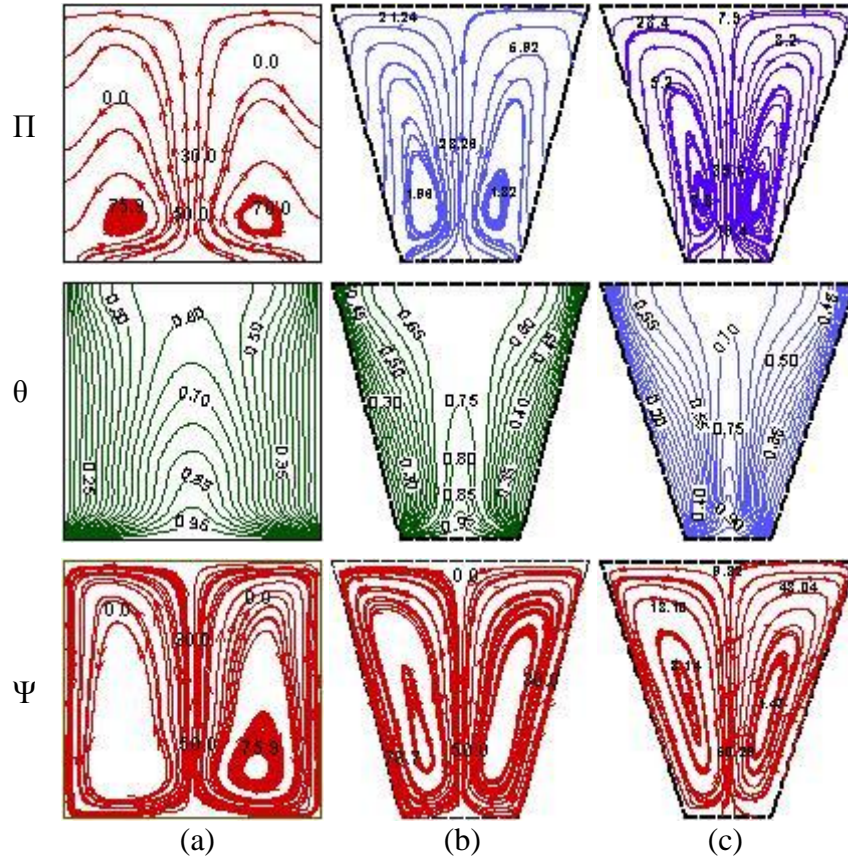


**Figure 3:** Stream function ( $\Psi$ ), temperature ( $\theta$ ), heat function or total heat flux( $\Pi$ ) contours for uniform bottom heating  $\theta(X,0) = 1$  with  $Pr = 0.026$ ,  $Ha = 50$  and  $Ra = 10^7$  (a)  $\Phi = 0^\circ$  (b)  $\Phi = 30^\circ$  (c)  $\Phi = 45^\circ$

Figure 4 exemplifies that the magnitudes of streamfunction are circular or elliptical near the core but the streamlines near the wall is almost parallel to wall exhibiting large intensity of flow for  $Pr = 0.7$  and  $Ra = 10^7$ . For  $Pr = 0.7$  and  $Ra = 10^7$  isotherms with  $\theta = 0.05 - 0.50$ ,  $\theta = 0.05 - 0.55$ ,  $\theta = 0.05 - 0.45$  occur symmetrically near the side walls of the enclosure and  $\theta \geq 0.55$ ,  $\theta \geq 0.60$ ,  $\theta \geq 0.50$  are smooth curves symmetric with respect to central symmetrical line for  $Ra = 10^7$ ,  $Pr = 0.7$  and  $\phi = 45^\circ, 30^\circ, 0^\circ$ (square cavity) respectively. Although streamlines are circular or elliptical near the core but streamlines near the wall are almost parallel to wall for intensity of flow (fig. 4). It is also fascinating that multiple correlations are absent for  $Pr = 0.7$  and  $Ra = 10^7$  whereas multiple heat circulation loops were observed for  $Pr = 0.026$  (fig. 3). Due to enhanced flow circulations the isotherms are highly compressed near the side walls except near the bottom wall especially for  $\phi = 45^\circ$  and  $30^\circ$ . The thermal energy is further analyzed with heatlines. The large

temperature gradient near the side walls are due to significant number of heatlines with a large variation of heat function as seen in figure 6a-c whereas the heatlines along the side walls are less dense leading to less thermal gradient and also near corners irrespective of  $\phi$  s.

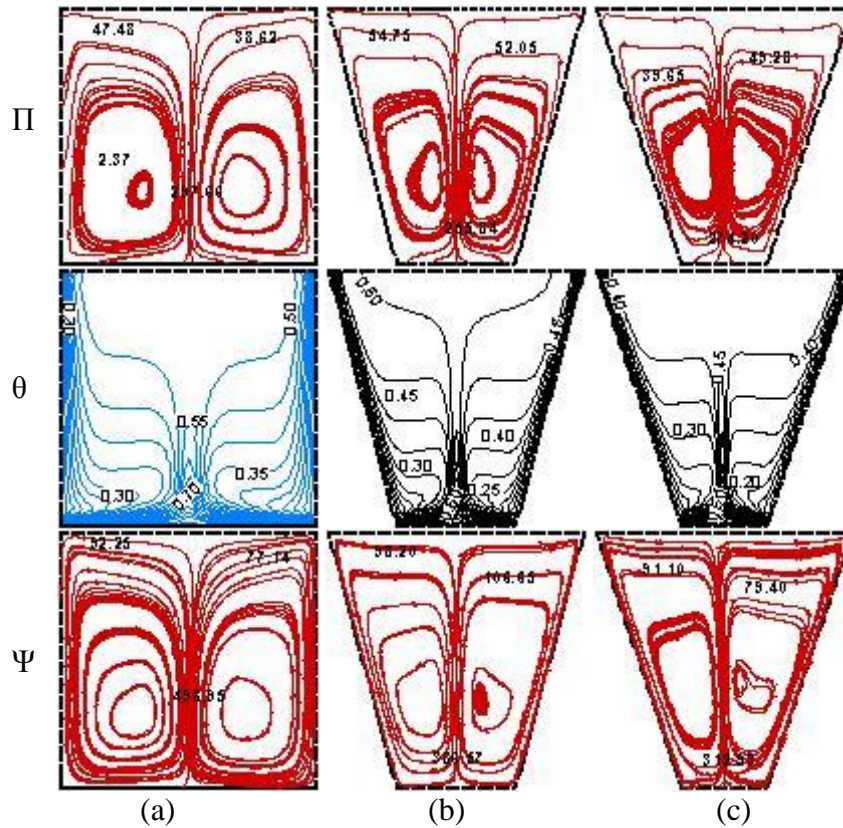


**Figure 4:** Stream function ( $\Psi$ ), temperature ( $\theta$ ), heat function or total heat flux( $\Pi$ ) contours for uniform bottom heating  $\theta(X,0) = 1$  with  $Pr = 0.7$ ,  $Ha = 50$  and  $Ra = 10^7$  (a)  $\Phi = 0^\circ$  (b)  $\Phi = 30^\circ$  (c)  $\Phi = 45^\circ$

Figure 5 shows streamline, Isotherms (temperature) and heatlines for  $Ra = 10^7$ ,  $Pr = 1000$  and  $\phi = 45^\circ, 30^\circ, 0^\circ$  (square cavity) respectively. For  $Pr = 1000$  and  $Ra = 10^7$  isotherms with  $\theta = 0.05 - 0.45$ ,  $\theta = 0.05 - 0.40$ ,  $\theta = 0.05 - 0.40$  occur symmetrically near the side walls of the enclosure and  $\theta \geq 0.50$ ,  $\theta \geq 0.45$ ,  $\theta \geq 0.45$  are smooth curves symmetric with respect to central symmetrical line for  $Ra = 10^7$ ,  $Pr = 1000$  and  $\phi = 45^\circ, 30^\circ, 0^\circ$  (square cavity) respectively. Comparative studies on figure 4 and figure 5 show that as  $Pr$  increases from 0.7 to 1000 for various  $Ra$ , the values of stream function on the core cavity increase because of highly viscous. It is exemplify that the greater circulations due to higher  $Pr$  leads to elliptical stream function in the core.

At larger  $Ra = 10^7$  and  $Pr = 1000$  (Fig. 5a-c), it is seen that the intensity of flow circulations are increased from the values of stream functions. Streamlines near the side walls take the shape of container or circular and signify enhance mixing effects.

## MHD Free Convection within Trapezoidal Cavity with Uniformly Heated Bottom

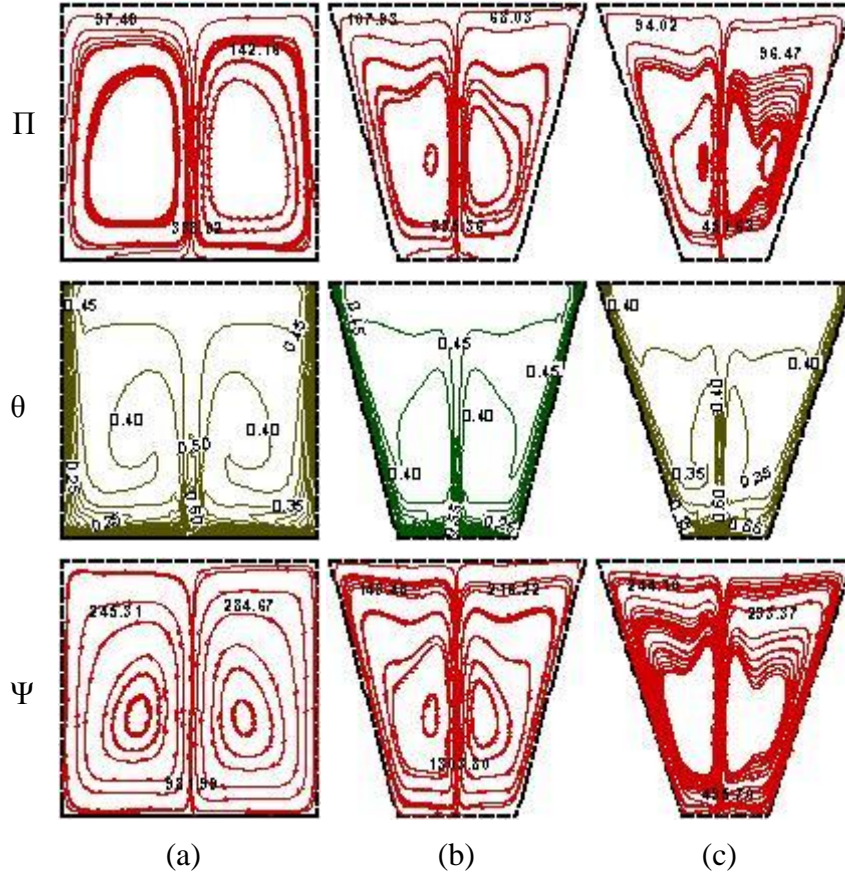


**Figure 5:** Stream function ( $\Psi$ ), temperature ( $\theta$ ), heat function or total heat flux( $\Pi$ ) contours for uniform bottom heating  $\theta(X,0) = 1$  with  $Pr = 1000$ ,  $Ha = 50$  and  $Ra = 10^7$  (a)  $\Phi = 0^\circ$  (b)  $\Phi = 30^\circ$  (c)  $\Phi = 45^\circ$

The isotherms  $\theta \leq 0.40$  are highly compressed near the side walls and isotherms with  $\theta \geq 0.50$  are also confined within a small regime near the bottom wall. The heatlines are highly dense at the central regime. It is also significant that at high  $Pr$  streamline except at the central regime is almost circular indicating higher intensity of flows. Also the significant numbers of heatlines are observed along the side walls leading to large thermal gradient for  $\phi = 45^\circ$  and  $30^\circ$  and heatlines are less dense along the side vertical walls. Besides, the effects of heat transfer for various  $Ra$  and inclination angles  $\phi = 45^\circ$ ,  $30^\circ$ ,  $0^\circ$  for different  $Pr$  on local and average Nusselt number are discussed later in detail.

### 7.2 Heat Transfer Rates: Local Nusselt Number vs distance and Average Nusselt Number vs Rayleigh Number

Figure 6(a) displays the effects of local Nusselt number vs distance for various inclinations of angles i.e. i)  $\phi = 0^\circ$ , ii)  $\phi = 30^\circ$ , iii)  $\phi = 45^\circ$ , for uniform heating of bottom wall with  $Pr = 0.026$ . Here the heat transfer rates are shown for  $Ra = 10^3$ . As

bottom wall is heated and side wall is cold and top wall is insulated so that for adjacent wall it is observed that heat transfer rate is maximum near edge of the left wall and the rate is step down from left side and it is straightly moving and then also it goes up to right side. Here the heat transfer rates are almost same for  $\phi = 30^\circ, 45^\circ$  except  $\phi = 0^\circ$  [square cavity]. Figure 6(a) also display similar effects of local Nusselt number with distance for various inclination tilt angles for  $Pr = 0.026$  in case of uniform heating. But here the values of heat transfer rate increase a little. Here the heat transfer rates are shown for  $Ra = 10^3, 10^4$ . Figure 6(a) also detects the variation of local Nusselt number with distance for various inclination tilt angles i.e. i)  $\phi = 0^\circ$ , ii)  $\phi = 30^\circ$ , iii)  $\phi = 45^\circ$ , with  $Pr = 0.026$  for uniform heating of bottom wall. Here heat transfer rates are discussed for  $Ra = 10^7$ . It is observed that heat transfer rates is very high at corners and it reduce the heat transfer rates toward the middle of bottom wall as the comparison of temperature contours is minimum at the center of wall irrespective of  $\phi$ s with  $Pr = 0.026$ .

Figure 6(b) shows the effects for various inclination angles when  $Ra = 10^3$  and  $Pr = 0.7$  in presence of uniform heating of bottom walls. Here the value of heat transfer rates increases as  $Pr$  increases. It is interesting to observe that the heat transfer rates ( $Nu_b$ ) for  $\phi = 30^\circ$ , and  $\phi = 45^\circ$  are almost identical except  $\phi = 0^\circ$ . It is also observed that thermal gradient is minimum at the center of bottom wall as seen from dispersed isotherm contours at the center of the wall for irrespective of  $\phi$ s. Figure 6(b) exemplify that similar effects of various inclination angles  $\phi = 45^\circ, 30^\circ, 0^\circ$  for  $Ra = 10^4, 10^5, 10^7$  with  $Pr = 0.7$  in presence of uniform bottom heating. Here, in case of uniform heating the heat transfer rate of left wall is very high and almost uniform near the bottom edge of hot vertical wall. As  $Ra$  increases then the magnitudes of heat transfer rates increases. But at larger  $Ra = 10^7$ , local heat transfer rates occur due to presence of secondary circulations which results isotherm contours at various places of bottom wall of uniform heating.

The heat transfer rates are also displayed in figure 7(a)-(c), where distributions of average Nusselt number of bottom wall respectively are plotted vs the logarithmic Rayleigh number. It may be noted that average Nusselt number is obtained by considering temperature gradient. It can also be noted that as  $Ra$  increases then the average Nusselt number increases. It is seen in figure 7(a) that as  $Ra$  increases from  $10^3$ - $10^6$  then average Nusselt number is straightly moving but as  $Ra$  increases more, then average Nusselt number is increasing for  $Pr = 0.026$ . As  $Pr$  increases (figure 7(b)) then conduction dominant heat transfer is narrowed down. It is also seen from figure 7(c), that, as  $Pr$  increases more, then from uniform heating case it is analyzed that average Nusselt number for bottom wall remain constant during the entire Rayleigh number regime. This illustrates the conduction dominant heat transfer for different Prandtl number regime irrespective of  $Ra$ .. It is observed that  $Nu_b$  at the middle portion of bottom wall for  $\Phi = 0^\circ$  is larger for uniform heating case whereas for  $\Phi = 30^\circ$  and  $45^\circ$  heat transfer rates are identical. It is also seen that  $Nu_s$  is largest near the bottom corner of side walls for  $\Phi = 0^\circ$ . At larges  $Pr$  ( $Pr=1000$ ) of uniform bottom heating it is seen that as  $Ra$  increase from  $10^3$  to  $10^6$ , then average heat transfer rates ( $Nu_b$ ) increases. After crossing  $Ra = 10^6$  then it is also seen average heat transfer rates are decreasing. After that when  $Ra$  goes to  $10^7$  then average heat transfer rate is also increasing because of highly viscous of  $Pr$ .

MHD Free Convection within Trapezoidal Cavity with Uniformly Heated Bottom

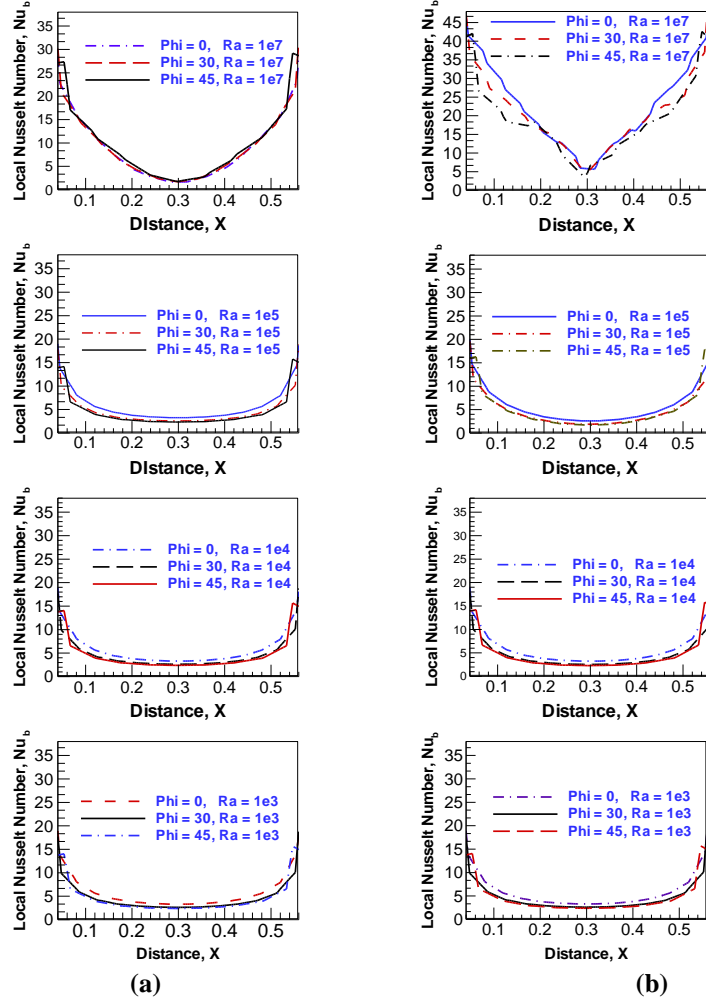


**Figure 6:** Variations of local Nusselt numbers ( $Nu_b$ ) with distance for a)  $Pr = 0.026$ , b)  $Pr = 0.7$  and  $Ra = 10^3, 10^4, 10^5, 10^7$  and for various inclination of angles  $\Phi = 0^\circ, 30^\circ, 45^\circ$  in presence of uniform heating of bottom walls.

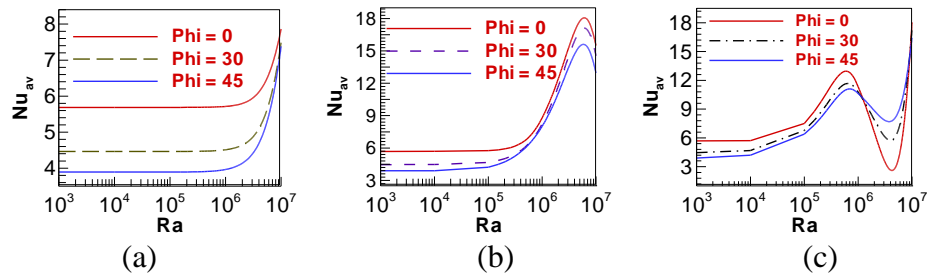


**Figure 7:** Variations of Average Nusselt Number vs Rayleigh number for (a)  $Pr = 0.026$ , (b)  $Pr = 0.7$ , (c)  $Pr = 1000$  and for various inclination of angles  $\Phi = 0^\circ, 30^\circ, 45^\circ$  in presence of uniform heating of bottom wall.

## 8. Conclusions

In this authentication, two-dimensional laminar steady state MHD free or natural convection within trapezoidal cavity for uniformly heated of bottom wall has been analyzed with heatlines concept by finite element method. The finite element equations were derived from the governing flow equations that consist of the conservation of mass, momentum, and energy equations. The derived finite element equations are nonlinear requiring an iterative technique solver. Galerkin weighted residual method has been applied to solve these nonlinear equations for solutions of the nodal velocity component, temperature, and pressure by considering Prandtl numbers of 0.026, 0.7, 1000, Hartman numbers of 50 and also Rayleigh numbers of  $10^3$  to  $10^7$ . The results show that,

1. The heat transfer rate is maximum near the edge of the wall and the rate is minimum near the center of the wall irrespective of all angles ( $\phi$ ) for uniform heating of the bottom wall for Rayleigh number  $10^3$  to  $10^7$  gradually.
2. The average Nusselt number ( $Nu$ ) at the uniform heating of bottom wall is the highest for the angle  $0^\circ$  when Rayleigh number  $10^7$ , whereas the lowest heat transfer rate for the angle  $45^\circ$  when Rayleigh number  $10^3$ . Moreover, the average Nusselt number, the uniform heated bottom wall is higher than those obtained with the non-uniform heated bottom wall for different angle.
3. Heat transfer depends on Prandtl number and heat transfer rate is maximum near the edge of the wall and the rate is minimum near the center of the wall irrespective of all angles ( $\phi$ ) for uniform heating of the bottom wall for different prandtl number.
4. The heat transfer rate average Nusselt Number,  $Nu_{av}$  increases with the increase of Rayleigh number, Ra, for uniform heating of bottom wall.

## Acknowledgements

The authors like to express their gratitude to the Department of Mathematics, Bangladesh University of Engineering and Technology, for providing computing facility during this work.

## REFERENCES

1. R. Anandalakshmi, T. Basak, Heat flow visualization for natural convection in rhombic enclosures due to isothermal and non-isothermal heating at the bottom wall, *International Journal of Heat and Mass Transfer*, 55 (2012), 13-25.
2. T. Basak, R. Anandalakshmi, Kumar Pushpendra, S. Roy, Entropy generation vs energy flow due to natural convection in a trapezoidal cavity with isothermal and non-isothermal hot bottom wall, *Energy*, 37 (2012), 514.
3. T. Basak, D. Ramakrishna, S. Roy, A. Matta, I. Pop, A comprehensive heatline based approach for natural convection flows in trapezoidal enclosures: Effect of various walls heating, *International Journal of Thermal Sciences*, 50, (2011) 1385.

#### MHD Free Convection within Trapezoidal Cavity with Uniformly Heated Bottom

4. T. Basak, S. Roy, A. Singh, A.R. Balakrishnan, Natural convection flows in porous trapezoidal enclosures with various inclination angles, *International Journal of Heat and Mass Transfer*, 52 (2009), 4612.
5. T. Basak, S. Roy, A. Singh, and B. D. Pandey, Natural convection flow simulation for various angles in a trapezoidal enclosure with linearly heated side wall(s), *International Journal of Heat and Mass Transfer*, 52 (2009), 4413.
6. T. Basak, S. Roy, S. K. Singh, and I. Pop, Finite element simulation of natural convection within porous trapezoidal enclosures for various inclination angles: Effect of various wall heating, *International Journal of Heat and Mass Transfer*, 52 (2009), 4135.
7. T. Basak, S. Roy, A. Singh, and I. Pop, Finite element simulation of natural convection flow in a trapezoidal enclosure filled with porous medium due to uniform and non-uniform heating, *International Journal of Heat and Mass Transfer*, 52 (2009), 70.
8. M. Boussaid, A. Mezenner, and M. Bouhadef, Convection naturelle de chaleur et de masse dans une cavité trapézoïdale, *International Journal of Thermal Sciences*, 38 (1999), 363.
9. M. Peric, Natural convection in trapezoidal cavities, *Num. Heat transfer A*, 24, (1993) 213.
10. E. Natarajan, T. Basak, and S. Roy, Natural convection flows in a trapezoidal enclosure with uniform and non-uniform heating of bottom wall, *International Journal of Heat and Mass Transfer*, 51 (2008), 747.
11. S. K. Natarajan, K.S. Reddy, and T. K. Mallick, Heat loss characteristics of trapezoidal cavity receiver for solar linear concentrating system, *Applied Energy*, 93 (2012), 523.
12. H. Saleh, R. Roslan, and I. Hashim, Natural convection in a porous trapezoidal enclosure with an inclined magnetic field, *Computers & Fluids*, 47 (2011), 155.
13. C. I. Hung, J. S. Tsai, and C. K. Chen, Nonlinear stability analysis of magnetohydrodynamic condensate film flow down a vertical plate with constant heat flux, *Int. J. Heat and Mass Transfer*, 39 (1996), 877.
14. T. Basak, S. Roy, and I. Pop, Heat flow analysis for natural convection within trapezoidal enclosures based on heatline concept, *Int. J. Heat Mass Transfer*, 52, (2009) 2471.
15. C. Taylor and P. Hood, A Numerical Solution of the Navier-Stokes Equations Using Finite Element Technique, *Computer and Fluids*, 73 (1973). doi:10.1016/0045-7930(73)90027-3.
16. P. Dechaumphai, *Finite Element Method in Engineering*, 2nd ed. Chulalongkorn University Press, Bangkok, 1999.